

- Clement, *Paleoceanography* **6**, 33 (1991).
4. J. C. Ingle Jr., in *The Monterey Formation and Related Siliceous Rocks*, R. E. Garrison and R. G. Douglas, Eds. (Society of Economic Paleontologists and Mineralogists, Los Angeles, CA, 1981), pp. 159–179.
 5. B. P. Flower and J. P. Kennett, *Geology* **21**, 877 (1993).
 6. D. J. De Paolo and K. L. Finger, *Geol. Soc. Am. Bull.* **103**, 112 (1991).
 7. C. M. Isaacs *et al.*, *U.S. Geol. Surv. Open-File Rep. 92-539-D* (1992), pp. 1–12.
 8. R. E. Garrison and R. G. Douglas, Eds., *The Monterey Formation and Related Siliceous Rocks* (Society of Economic Paleontologists and Mineralogists, Los Angeles, CA, 1981).
 9. The geologic map is from C. M. Isaacs [in (8), p. 257], who used maps from T. W. Dibblee Jr. [*Calif. Div. Mines Geol. Bull.* **186**, 1 (1966)].
 10. C. M. Isaacs, *Geol. Soc. London Spec. Publ.* **15** (1984), p. 481.
 11. _____ and J. Rullkötter, Eds., *AAPG Stud. Geol. Ser.*, in press.
 12. A. Schimmelmann *et al.*, in (11).
 13. For detailed sample preparation procedures see (14). Before isotopic analysis, *N*-alkanes were removed by molecular sieving (5A). Carbon isotope values are reported as $\delta^{13}\text{C} = 10^3[(\text{R}_x - \text{R}_s)/\text{R}_s]$, where R = $^{13}\text{C}/^{12}\text{C}$, and x and s designate the sample and the PDB standard, respectively. Individual compound isotope analyses were performed on a GC-C-MS system (14) with some modifications of the analytical configuration and procedures (14–17).
 14. S. Schouten, M. Schoell, J. S. Sinninghe Damsté, R. E. Summons, J. W. de Leeuw, in (11).
 15. J. M. Hayes, K. H. Freeman, B. N. Popp, C. H. Hoham, *Org. Geochem.* **16**, 1115 (1990).
 16. M. Schoell, M. A. McCaffrey, F. J. Fago, J. M. Moldowan, *Geochim. Cosmochim. Acta* **56**, 1391 (1992).
 17. B. R. T. Simoneit, M. Schoell, R. F. Dias, F. R. De Aquino Neto, *ibid.* **57**, 4205 (1993).
 18. D. J. Hollander, S. G. Wakeham, J. M. Hayes, written communication.
 19. M. E. L. Kohnen, J. S. Sinninghe Damsté, J. W. de Leeuw, *Nature* **349**, 775 (1991).
 20. M. J. DeNiro and S. Epstein, *Science* **197**, 261 (1977).
 21. B. D. Fry and S. C. Wainright, *Mar. Ecol. Prog. Ser.* **76**, 149 (1991).
 22. G. Ourisson *et al.*, *Pure Appl. Chem.* **51**, 709 (1979).
 23. M. Rohmer *et al.*, in *Biological Markers in Sediments and Petroleum*, J. M. Moldowan *et al.*, Eds. (Prentice-Hall, Englewood Cliffs, NJ, 1991), pp. 1–17.
 24. S. Emerson, *Geophys. Monogr. Am. Geophys. Union* **32**, 78 (1985).
 25. J. W. Collister *et al.*, *Org. Geochem.* **19**, 265 (1992).
 26. R. O. Olson, S. W. Chrisholm, E. R. Zettler, M. Altabet, J. Dusenberry, *Deep Sea Res.* **37**, 1033 (1990).
 27. S. W. Chrisholm *et al.*, *Arch. Microbiol.* **157**, 297 (1992).
 28. K. H. Freeman and J. M. Hayes, *Global Biogeochem. Cycles* **6**, 185 (1992).
 29. R. Goericke, J. P. Montoya, B. Fry, in *Stable Isotopes in Ecology*, K. Laijtha and B. Michener, Eds. (Blackwood Scientific, London, in press).
 30. The fractionation ϵ_s in Eq. 1 is similar but not identical. The C_{35} hopanes contain all 30 carbons of the acetate-derived squalene precursor plus five from the ribose side-chain moiety (M. Rohmer *et al.*, *J. Chem. Soc. Chem. Commun.* **1989**, 1471 (1989)). Cholestane contains 27 carbon atoms derived exclusively from squalene. Consequently, sulfur-bound hopanes are expected to be incrementally enriched in ^{13}C because of the presence of 5/35 carbohydrate-derived carbon atoms. Because the hopanes are consistently ^{13}C -depleted with respect to steranes, the difference between the $\delta^{13}\text{C}$ signatures of steranes and hopanes tends to underestimate marginally the differences arising from factors controlling photosynthetic fractionation. Although the isotopic differences between the squalene-derived pentacyclic nucleus and the side chain of a hopane have not yet been measured, we estimate that the total effect should be on the order of 1 per mil or less.
 31. In natural populations of algae and cyanobacteria, individual sterols and hopanols have isotopic compositions similar to, or slightly depleted with respect to, those of the crude lipid fractions from which they are prepared and are depleted by 3 to 6 per mil compared to total biomass (R. E. Summons, unpublished results).
 32. P. M. Kroopnick, *Deep Sea Res.* **32**, 57 (1985).
 33. A. P. McNicol and E. R. M. Druffel, *Geochim. Cosmochim. Acta* **56**, 3589 (1992).
 34. W. Kuspert, in *Cyclic and Event Stratification*, G. Einsele and A. Seilacher, Eds. (Springer, Berlin, 1982), p. 482; D. J. Hollander *et al.*, *Global Biogeochem. Cycles* **7**, 157 (1993).
 35. Short-term ^{13}C depletions in calcites of benthic foraminifera in the Naples Beach profile around 14 Ma [figure 1 in (5)] are on the order of 1 to 2 per mil and are related to short-term ^{13}C fluctuations in sedimentary ^{13}C (B. P. Flower, personal communication).
 36. R. Francois *et al.*, *Global Biogeochem. Cycles* **7**, 627 (1993).
 37. G. H. Rau, T. Takahashi, D. J. Des Marais, *Nature* **341**, 516 (1989).
 38. G. H. Rau, T. Takahashi, D. J. Des Marais, C. W. Sullivan, *J. Geophys. Res.* **96**, 15131 (1991).
 39. J. D. Wright *et al.*, *Paleoceanography* **7**, 357 (1992).
 40. S. M. Savin *et al.*, *Mar. Micropaleontol.* **6**, 423 (1981).
 41. F. Woodruff, S. M. Savin, R. G. Douglas, *Science* **212**, 665 (1981).
 42. E. Barrera *et al.*, *Geol. Soc. Am. Mem.* **163**, 83 (1985).
 43. S. M. Savin *et al.*, *ibid.*, p. 49.
 44. K. G. Miller *et al.*, *J. Geophys. Res.* **96**, 6829 (1991).
 45. We thank D. J. Hollander, S. Wakeham, and J. M. Hayes for use of unpublished data from their Santa Monica Bay study; numerous contributors of the Cooperative Monterey Organic Geochemistry Study project, in particular C. M. Isaacs and A. Schimmelmann for release of information to us before publication; and J. M. Hayes, K. H. Freeman, M. A. McCaffrey, J. P. Kennett, B. P. Flower, J. D. Wright, and R. Goericke for helpful input. Supported by a PIONEER grant (J.S.S.D.) from the Netherlands Organization for Scientific Research and by the Chevron Petroleum Technology Company, whom we thank for permission to publish. This is Netherlands Institute of Sea Research Marine Biogeochemistry contribution No. 292.

22 June 1993; accepted 23 November 1993

Deep, Zonal Subequatorial Currents

Lynne D. Talley* and Gregory C. Johnson

Large-scale, westward-extending tongues of warm (Pacific) and cold (Atlantic) water are found between 2000 and 3000 meters both north and south of the equator in the Pacific and Atlantic oceans. They are centered at 5° to 8° north and 10° to 15° south (Pacific) and 5° to 8° north and 15° to 20° south (Atlantic). They are separated in both oceans by a contrasting eastward-extending tongue, centered at about 1° to 2° south, in agreement with previous helium isotope observations (Pacific). Thus, the indicated deep tropical westward flows north and south of the equator and eastward flow near the equator may result from more general forcing than the hydrothermal forcing previously hypothesized.

The upper ocean circulation is known to be vigorous and basically east-west in orientation, but despite many years of oceanographic observation of the tropical Pacific, relatively little is known about the circulation below a depth of about 1000 m. More is known about the deep tropical Atlantic circulation because of its strong water mass signatures in temperature, salinity, oxygen, and nutrients. In the Pacific the discovery of helium tongues of hydrothermal origin has resulted in the hypothesis that the dominant large-scale tropical circulation centered at about 2500 m depth consists of westward flow in two broad bands north and south of the equator (1). Recent detailed and large-scale observations made as part of the World Ocean Circulation Experiment

(WOCE) and South Atlantic Ventilation Experiment are allowing the detailed description of the major elements of the circulation at these depths. In this report, evidence of longitudinally extensive east-west flows at these depths within 15° to 20° of the equator is presented, as indicated in the fields of temperature, salinity, and oxygen measured with unprecedented latitudinal resolution; similarity between flow patterns that have been hypothesized for the Pacific and Atlantic is demonstrated.

The existence of large-scale zonal flow at depth in the South Pacific is well known because of its hydrothermal signature. Plumes of water with high $^3\text{He}/^4\text{He}$ ratios emitted from the East Pacific Rise at 15°S (2) were observed along 125°W, 135°W, and the dateline (1, 3), in a core centered at 2500 m at 15° to 20°S. Upward motion from hydrothermal sources directly over the rise that feeds the warm, helium-rich tongue extending to the west was demonstrated by Hautala and Riser (4). The South Pacific plume is also evident in maps

L. D. Talley, Scripps Institution of Oceanography, University of California, San Diego, La Jolla, CA 92093-0230, USA.

G. C. Johnson, Pacific Marine Environmental Laboratory, National Oceanic and Atmospheric Administration, Seattle, WA 98115, USA.

*To whom correspondence should be addressed.

of potential temperature and salinity (5). A North Pacific helium plume at 5° to 10°N was also apparent in the early observations at 125°W and the dateline (3) and has since been observed in more detail by Craig at 135°W (5) and by Jenkins at 10°N (6). Craig concluded that the source of the North Pacific ³He maximum was also the East Pacific Rise, between 5° and 10°N (1). Both Pacific plumes are also characterized by marked temperature (1), silica, oxygen, potential vorticity, and velocity shear signatures. As a result of the South Pacific ³He observations, Stommel suggested (7) that hydrothermal venting on the East Pacific Rise forced westward jets at mid depths. Alternatively, he suggested that general abyssal thermohaline circulation (8) is augmented with strong local hydrothermal forcing (9).

Primary temperature and salinity data from WOCE meridional hydrographic sections at 135°W (Fig. 1) and 151°W, which were made in June to September 1991 aboard the research vessel *Thomas Washington*, reveal these zonal features in the Pacific Ocean. Data from a section at ~125°W, made in 1971 (10), complement the new data. The data show that the shallower isopycnals are depressed from 20° toward 5° to 7° on both sides of the equator and form a bulge upward at the equator. In contrast, deeper isopycnals are elevated toward the equator and bulge downward at the equator. The deepest isopycnals are elevated to their shallowest point at the equator.

Potential temperature on isopycnals at depths of 2000 to 4000 m shows large-scale warm and cold anomalies (Figs. 2 and 3). On the largest scale, warm (salty) waters are in the south and in the tropics, whereas colder (fresher) waters reside in the subtropical South Pacific and in the northern North Pacific. The warm southern waters are produced by the mixing of the relatively saline North Atlantic deep water (NADW) into the circumpolar deep water (CPW) of the Antarctic circumpolar current. All low temperature and salinity on the isopycnal must be produced by vertical diffusion, because the only lateral source of water is the Antarctic (5). The colder, fresher water in the North Pacific is also oxygen-poor and silica-rich and is known as Pacific deep water; it has no surface source there. On a smaller scale, a double lobe of high-temperature waters spans the equator on all isopycnals from 36.92 to 37.02σ₂. The highest temperatures at 135°W (Fig. 3B) are in two separate regions, centered at 12°S and 6°N and at 36.96 to 36.98σ₂ (2700 to 2900 dbar). The temperature anomalies decrease above and below this range and are not apparent at 36.80σ₂ (1800 dbar, not shown) or near the bottom at 37.04σ₂. This pattern corresponds well with that observed in ³He/⁴He ratios (1,

3). The peak temperature south of the equator is higher than that north of the equator, perhaps because both warm tongues originate in the south as CPW or because a hydrothermal heat source for the southern tongue is more intense. The minimum in the temperature profile between the two lobes is slightly south of the equator, between 1° and 3°S.

At 151°W (Fig. 3A), the pattern is similar and the highest temperatures relative to the background are at 36.96 to 36.98σ₂. The highest temperatures here are at 8° both north and south of the equator. The pattern at 125°W (Fig. 3C) is more difficult to discern, but it too has maximum temperature anomalies at 36.96 to 36.98σ₂, located asymmetrically about the equator at

12°S and 7° to 8°N, with a minimum temperature also at about 2°S. The double-lobed structure is not apparent east of the East Pacific Rise (for example, Fig. 3D).

To determine the lateral extent of the deep tropical temperature structure, we mapped the potential temperature at 36.96σ₂ for the Pacific (Fig. 2). The isopycnal depth is near 2600 m in the tropical Pacific. We used all currently available WOCE conductivity, temperature, and depth (CTD) sections, several well-sampled pre-WOCE CTD sections, and a selection of high-quality bottle data. The South Pacific warm tongue is defined clearly by the historical data including the 125°W Geosecs section and is apparent on Reid's map of salinity at 2500 m (5). The warm tongue in the North Pacific contrasts

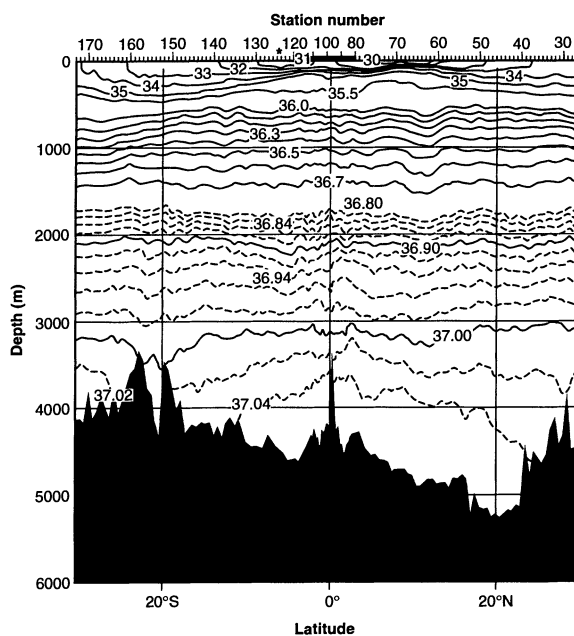
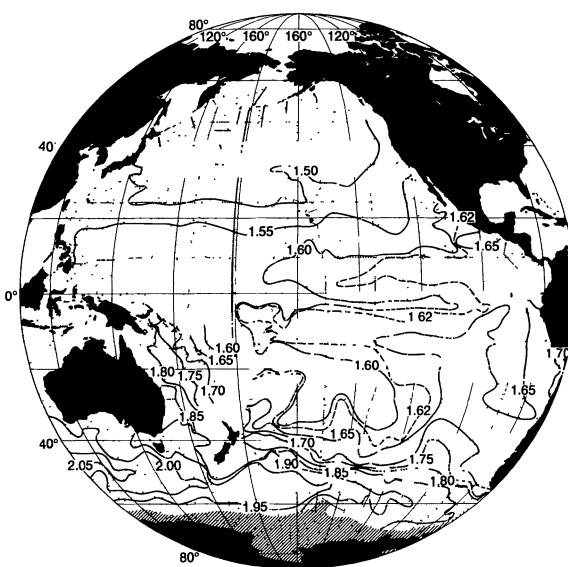


Fig. 1. Potential density anomaly referenced to 2000 dbar (σ_2 values are shown in units of kilograms per cubic meter), nominally along 135°W in the Pacific (WOCE P17). Isopycnals below 2000 m slope down from 20° to between 5° and 7° on either side of the equator and bulge upward at the equator. The 151°W section has similar features.

Fig. 2. Map of potential temperature (in degrees Celsius) at 36.96σ₂, interpolated vertically from discrete data with the use of a cubic spline. The densely sampled sections at 150° to 155°W, 135°W, and 85° to 88°W and the line of stations at about 125°W are the four sections used in Fig. 3. The error is approximately 0.02°C, arising primarily from differences in standard sea waters used for the calibration of salinity. Some attempt was made to correct for this bias. Important contoured features are identifiable in individual data sets, for which the error is less than 0.01°C. The warm tongues on either side of the equator extend westward from the East Pacific Rise at 5° to 8°N and 10° to 15°S. A zonal cold tongue is located slightly south of the equator. The relatively warm water in the Antarctic is circumpolar deep water, and the relatively cold water in the North Pacific is Pacific deep water.



less with the background (also seen in Fig. 3).

The two warm tongues appear to extend westward from the warmest pools in the eastern Pacific north and south of the equator. These correspond with the high ³He features found by Craig (1). Two meridional warm tongues extend northward in the eastern South Pacific, one just east of the East Pacific Rise and one along the South American coast; they are separated by a southward-extending cold tongue. Whether the main source of heat for the two zonal plumes is the East Pacific Rise or, instead, the Southern Ocean (for the South Pacific plume) and the eastern boundary (for the North Pacific plume) is not clear from these data. The narrow cold feature just south of the equator extends eastward from near the western boundary and may be supplied either by the colder Pacific deep water of the North Pacific, the cold center of the anticyclonic gyre in the western South Pacific through a western boundary current that is very narrow between 8° and 15°S, or by local upwelling.

These features substantiate, with greater spatial resolution and lateral extension, Craig's hypothesis (1) from ³He data of a pattern in which flow is westward in the warm tongues at 10° to 12°S and 5° to 10°N and eastward at 1° to 3°S. Firing's direct current measurements (11) along 159°W from 3°N to 3°S, averaged over 16 months, show that the most energetic flow below

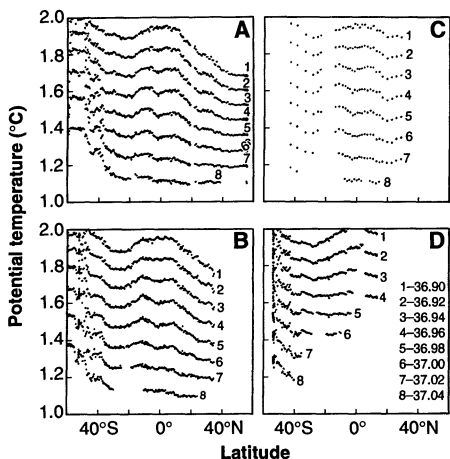


Fig. 3. Potential temperature (in degrees Celsius, CTD) on surfaces of potential density referenced to 2000 dbar, σ_2 , at (A) 151°W (WOCE P16 south of Hawaii, July to September 1991; north of Hawaii, May to June 1984), (B) 135°W (WOCE P17, June to July 1991), (C) 125°W (Geosecs, April to May 1974), and (D) 85° to 88°W (WOCE P19, January to April 1993). In each panel, the topmost (warmest) isopycnal is $\sigma_2 = 36.90 \text{ kg m}^{-3}$. Isopycnals are shown in (D) as multiples of σ . The depth range is 2000 to 4000 m (see Fig. 1). Warm anomalies are present at 5° to 8°N and 10° to 15°S in all sections (suggesting westward flow), separated by a cold region centered at 2°S (suggesting eastward flow).

2000 m is eastward at 2.5 cm/s between 2600 and 3000 m, centered at 2°S, consistent with the location of the cold tongue (Fig. 2). The South Pacific part of this pattern is similar to Reid's adjusted geostrophic circulation at 2500 m (5).

Flows similar to those of the tropical Pacific are evident in the tropical Atlantic. Like the Pacific, the Atlantic has two thick water masses in this depth range: NADW and CPW. NADW has higher salinity and oxygen than CPW; its high salinity originally arises from the Mediterranean Sea, and its high oxygen arises from the Labrador Sea and Arctic Ocean. CPW contains a component of NADW that has circulated southward through the South Atlantic to the Southern Ocean and then around Antarctica, where its salinity is lowered by mixing with waters of Antarctic and North Pacific origin. The oxygen of CPW is lowered by age and by admixture of oxygen-poor Indian and Pacific waters. The large-scale horizontal intermingling of NADW and CPW in the Atlantic results in lateral variations in salinity and oxygen on isopycnals (12, 13).

In the South Atlantic, NADW spreads southward along the western boundary and CPW spreads northward in the eastern part of the ocean (13-15). Salinity and oxygen on isopycnals, ranging from 36.80 to 37.04 σ_2 (1400 to 3000 m between 20°S and 40°N), show alternating east-west tongues of NADW and CPW (12-14). On Reid's maps (13), a tongue of low salinity and low oxygen CPW extends westward in the North Atlantic centered at 5° to 10°N; a tongue of high salinity in the upper NADW and high oxygen in the middle and lower NADW extends eastward near the equator; a tongue of low salinity and high oxygen extends westward in the South Atlantic between 8° and 20°S. The eastward flow of upper NADW along the equator was

demonstrated in Weiss's measurements of chlorofluorocarbons (15); only the upper NADW contains measurable CFCs, indicating that it is the most recently ventilated of these waters.

At 25°W (Fig. 4), depressions in salinity and oxygen indicating westward flow are found, one north of the equator at 5° to 8°N and two south of the equator at 5° to 8°S and at 12° to 18°S; the 5° to 8°S tongue is not apparent in most data sets but is a strong feature on the 25°W section. The Atlantic signatures of zonal flow are less dramatic than those in the Pacific, possibly because they are obscured by the large-scale trend from waters with low salinity and high oxygen in the Southern Ocean to waters with high salinity and low oxygen just below the Mediterranean tongue at about 30°N. There is remarkable horizontal and vertical homogeneity in salinity and oxygen between 16°S and 13°N; the interleaving CPW and NADW signatures are weakly imposed, as if the region is somewhat isolated from the gyres to the north and south except for a small amount of newer CPW and NADW swirled in, delineating the tongues under discussion.

As in the Pacific, these tongues are the primary large-scale features of salinity and oxygen between 20°S and 15°N. If flow were along the axes of the tongues, rather than around them, westward flow would be indicated at 5° to 8°N (5° to 8°S) and 12° to 18°S, and eastward flow at 8° to 12°S and at 1° to 2°S. The similarity of structures in the thick deep-water layers in the Pacific and Atlantic oceans and the near symmetry between Northern and Southern hemisphere flows in both the Pacific and Atlantic suggest that the forcing mechanism is general rather than specific to one region.

The Stommel and Arons model (8), which provides our basic understanding of

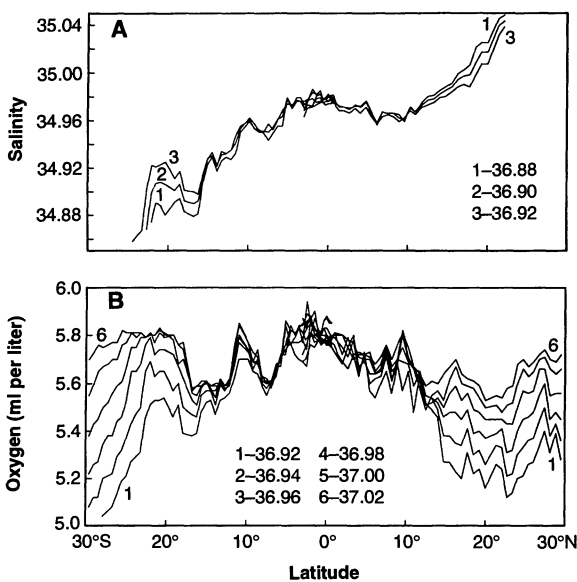


Fig. 4. (A) Salinity and (B) oxygen on surfaces of uniform potential density anomaly relative to 2000 dbar at 25°W in the Atlantic Ocean (July to September 1988 for 3°S to 63°N; January to April 1989 for 54°S to 1°N). Isopycnals are shown as multiples of σ . The depth range is 1600 to 2700 m. The salinity pattern in the Pacific is reversed in the Atlantic; in both oceans the off-equatorial, westward-extending tongues are of CPW, which is fresh in the Atlantic and salty in the Pacific relative to the deep waters from the Northern Hemisphere in each ocean.

abyssal circulation, on the assumption of a flat-bottomed ocean driven by uniform upwelling, predicts that flow is poleward and eastward throughout the interior ocean. However, in both the Pacific and Atlantic, the westward-extending tongues have the proper characteristics for CPW, which thus spreads equatorward from the Southern Ocean in the eastern South Pacific and South Atlantic. Thus, if the Stommel and Arons model were appropriate, the westward flow we observe would have to lie above the maximum in deep upwelling (16). The equatorial tongues, which suggest eastward flow, have been well-documented in the Atlantic (12–15); Böning and Schott's recent model (17) suggests that a kelvin wave mechanism can produce such a current and its slight southward shift relative to the equator. A second model that has been suggested for the South Pacific warm tongue is hydrothermal forcing from the East Pacific Rise (7, 9). Hydrothermal heating probably increases the temperature of waters in the eastern Pacific, although vertical diffusion also may be effective in spreading heat and salt downward in the tropics. The stronger signature of the warm tongue in the South Pacific relative to the North Pacific may be the result of asymmetric thermal forcing from the ridge crests. However, hydrothermal forcing is not likely the sole forcing mechanism for these deep low-latitude flows because there is no hydrothermal signature in the Atlantic.

REFERENCES AND NOTES

1. H. Craig, *Eos* 71, 882 (1990); *ibid.*, p. 1396; *ibid.* 72, 491 (1991). The first two of these abstracts reports high $^3\text{He}/^4\text{He}$ cores along 135°W, centered at 11°30'S (2400 m depth) and 7°30'N (2600 m depth); the lowest $^3\text{He}/^4\text{He}$ ratio in this depth range is at 2°30'S. It was hypothesized that the high ^3He cores indicate westward flow at the cores and the intervening low ^3He core, eastward flow. In the third abstract observations were reported of two hydrothermal vents with high $^3\text{He}/^4\text{He}$ on the East Pacific Rise in the North Pacific; the conclusion was that these are the source of the high $^3\text{He}/^4\text{He}$ observed at 125°W (3) and 135°W.
2. J. E. Lupton and H. Craig, *Science* 214, 13 (1981).
3. H. G. Ostlund, H. Craig, W. S. Broecker, D. Spencer, *Geosecs Atlantic, Pacific, and Indian Ocean Expeditions* (National Science Foundation, Washington, DC, 1987), vol. 7.
4. S. L. Hautala and S. C. Riser, *J. Phys. Oceanogr.* 23, 1975 (1993).
5. J. L. Reid, *Prog. Oceanogr.* 16, 1 (1986).
6. W. J. Jenkins, *Oceanus* 35, 47 (1993).
7. H. Stommel, *Earth Planet. Sci. Lett.* 61, 63 (1982).
8. _____ and A. B. Arons, *Deep Sea Res.* 6, 140 (1960).
9. S. L. Hautala and S. C. Riser, *J. Phys. Oceanogr.* 19, 596 (1989).
10. H. Craig, W. S. Broecker, D. Spencer, *Geosecs Pacific Ocean Expedition* (National Science Foundation, Washington, DC, 1981), vol. 4.
11. E. Firing, *J. Geophys. Res.* 94, 2023 (1989).
12. M. Tsuchiya, L. D. Talley, M. S. McCartney, *Deep Sea Res.* 39, 1885 (1992); *J. Mar. Res.*, in press.
13. J. L. Reid, *Prog. Oceanogr.* 23, 149 (1989).
14. G. Wüst, *Wiss. Ergeb. Deutschen Atl. Exped. Forsch. Vermess. Meteor 1925–1927* 6, 109

- (1935); J. L. Reid, *Prog. Oceanogr.* 33, 1 (1994).
15. R. F. Weiss, J. L. Bullister, R. H. Gammon, M. J. Warner, *Nature* 314, 608 (1985); R. F. Weiss, M. J. Warner, K. G. Harrison, *Eos* 69, 1132 (1989).
16. M. E. Fiadeiro, *J. Mar. Res.* 40, 537 (1982); K. Speer, *Deep Sea Res.* 40, 925 (1992); B. A. Warren and G. C. Johnson, *Mar. Geol.* 104, 279 (1992).
17. C. W. Böning and F. A. Schott, *J. Geophys. Res.* 98, 6991 (1993).
18. M. Tsuchiya collected the tropical 135°W data, and J. Swift provided data comprising the southern parts of 151°W and 135°W; M. McCartney and M. Tsuchiya were co-investigators for the 25°W section. We thank B. Taft, J. Toole, G. Roden, J. Reid, J. Bullister, and J. Swift for generously

providing other recent Pacific data; H. Craig for providing a preliminary version of the $^3\text{He}/^4\text{He}$ section at 135°W; and Scripps Institution of Oceanography Oceanographic Data Facility and Woods Hole Oceanographic Institution's CTD group for providing technical support for 25°W, 135°W, and 151°W. Supported by WOCE funding from the Ocean Sciences Division of the National Science Foundation to Scripps Institution of Oceanography [OCE89-18961, OCE90-04394 (L.D.T.)], the National Oceanic and Atmospheric Administration (NOAA) Office of Global Programs (G.C.J.), and contribution 1500 from NOAA Pacific Marine Environmental Laboratory.

26 August 1993; accepted 3 December 1993

Extension of Life-Span by Overexpression of Superoxide Dismutase and Catalase in *Drosophila melanogaster*

William C. Orr and Rajindar S. Sohal

The hypothesis that oxygen free radicals are causally involved in the aging process was tested by a study of the effects of simultaneous overexpression of copper-zinc superoxide dismutase and catalase. As compared to diploid controls, transgenic flies carrying three copies of each of these genes exhibited as much as a one-third extension of life-span, a longer mortality rate doubling time, a lower amount of protein oxidative damage, and a delayed loss in physical performance. Results provide direct support for the free radical hypothesis of aging.

Although numerous hypotheses have been advanced, the nature of the causal mechanisms underlying the aging process is poorly understood and is a subject of intense debate. One hypothesis suggests that oxygen free radicals and hydroperoxides, collectively termed reactive oxygen species (ROS), are causal factors in aging (1). Reactive oxygen species are initially produced by the univalent reduction of dioxygen to generate sequentially superoxide anion radical and hydrogen peroxide. The latter, if not eliminated, generates the highly reactive hydroxyl free radical, which is widely believed to be the main agent of oxidative damage (2). The main assumption of the free radical hypothesis of aging is that the normal level of antioxidant defenses is not fully efficient, so that a fraction of ROS escape elimination. These ROS inflict molecular damage, some of which is irreparable and accumulates with age, thereby causing functional attrition associated with aging. Although this hypothesis is intuitively appealing, as a result of the ubiquitous generation of the potentially deleterious ROS, a direct causal link between ROS and aging has not been established.

If ROS are indeed a causal factor in aging, the enhancement of the defenses against ROS should reduce oxidative stress, decrease the

rate of aging, and extend life-span. The present study tests the predictions of the free radical hypothesis by the examination in *Drosophila melanogaster* of the effect of the overexpression of Cu-Zn superoxide dismutase (SOD) and catalase genes, which, acting in tandem, provide the primary enzymatic antioxidant defenses. Superoxide dismutase converts superoxide anion radical to H_2O_2 , and catalase breaks down H_2O_2 into water and oxygen, thus eliminating the possibility of the production of the highly reactive hydroxyl free radical. Because glutathione peroxidase, another enzyme involved in H_2O_2 removal, is absent in insects (3), SOD and catalase constitute the first coordinated unit of defense against ROS. The simultaneous overexpression of Cu-Zn SOD and catalase in an isogenic background was found to extend the life-span and slow down various age-related biochemical and functional alterations in *Drosophila melanogaster*.

Before the construction of transgenic lines overexpressing both Cu-Zn SOD and catalase, *Drosophila* lines bearing extra copies of SOD alone and catalase alone were created in an isogenic background (4). To generate flies with one extra copy of the SOD gene and one extra copy of the catalase gene, as well as control flies with two vector-only inserts, transgenic lines were first made heterozygous for dominantly marked balancer chromosomes (5). Appropriate heterozygotes were allowed to mate

Department of Biological Sciences, Southern Methodist University, Dallas, TX 75275, USA.